Domain Decomposition for Reservoir Flow Problems

Ove Sævareid*
Helge K. Dahle*
Magne S. Espedal*

Abstract. Using an operator-splitting technique based on the modified method of characteristics, [5], the saturation equation for two-phase immiscible flow in porous media leads to a nonsymmetric bilinear form. Addressing this problem via a Petrov-Galerkin finite-element-method, we discuss dynamic local grid refinement and choice of appropriate trial and testfunctions. A preconditioner based on ideas of Bramble et.al [2],[3] is proposed for the resulting non-symmetric linear system. We also consider the pressure equations. Here we introduce an approach aiming at the construction of accurate, consistent and piecewise linear velocity components from a piecewise linear pressure approximation. Computational results for a two dimensional model are presented.

1 Introduction.

Neglecting gravity and compressibility, two-phase immiscible flow in a porous media can be described by the set of partial differential equations:

$$\nabla \cdot \mathbf{v} = q_1(\mathbf{x}, t), \tag{1}$$

$$\mathbf{v} = -\mathbf{A}(S, \mathbf{x}) \cdot \nabla p, \tag{2}$$

$$\phi \frac{\partial}{\partial t} S + \nabla \cdot (f(S)\mathbf{v}) - \epsilon \nabla \cdot (\mathbf{D}(S, \mathbf{x}) \cdot \nabla S) = q_2(\mathbf{x}, t), \tag{3}$$

where $\mathbf{v}$ is the total Darcy velocity, p the total fluid pressure, S denotes the saturation of water and ϵ is a parameter scaling the diffusion term. We restrict ourselves to two space dimensions and assume the absolute permeability tensor to have the form

$$\mathbf{K}(\mathbf{x}) = k_x(\mathbf{x})\mathbf{ii} + k_y(\mathbf{x})\mathbf{jj}. \tag{4}$$

Let λ_i, $i = w, o$ denote the mobility of water and oil respectively. We then have

*Department of Applied Mathematics, University of Bergen, Allegt. 55, N5007 Bergen, Norway.

$$\mathbf{A}(S,\mathbf{x}) = \mathbf{K}(\mathbf{x})(\lambda_w + \lambda_o), \tag{5}$$

$$f(S) = \frac{\lambda_w}{\lambda_w + \lambda_o}, \tag{6}$$

$$\mathbf{D}(S,\mathbf{x}) = \mathbf{K}(\mathbf{x})\frac{\lambda_w\lambda_o}{\lambda_w + \lambda_o}\frac{dp_c}{dS}, \tag{7}$$

where p_c is the capillary pressure. The mobilities and the capillary pressure are assumed to be known functions of the water saturation.

In order to specify a concrete computational problem, we need boundary and initial conditions. The repeated five-spot well pattern is frequently used as a test case for these equations. In this context, it is natural to impose the boundary conditions

$$\mathbf{v}\cdot\mathbf{n} = 0, \quad \mathbf{x}\in\partial\Omega \tag{8}$$

$$\nabla S\cdot\mathbf{n} = 0, \quad \mathbf{x}\in\partial\Omega \tag{9}$$

where Ω is our computational domain and $\mathbf{n}$ denotes the unit normal out of Ω.

We shall adopt a sequential solution strategy to handle the system (1) - (3). Assuming a weak saturation dependency in equations (1) - (2), one solves for the pressure and velocity using the saturation at the present time. The velocity field is then assumed to be known when we advance the saturation to the next time level using equation (3).

2 Pressure and Velocity.

Given the saturation, S, the equations (1)-(2) constitute a saddle point problem for pressure and velocity. We may, of course, solve these equations simultaneously using a mixed finite element method, [9]. However, we will here consider a more classic approach. Eliminating the velocity between eqs. (1)-(2) leaves us to solve a second order elliptic equation for the pressure. The weak formulation for this problem is

$$A(p,\phi) = (q_1,\phi), \tag{10}$$

where $A(u,v) = \iint_\Omega \mathbf{A}\cdot\nabla u\cdot\nabla v\,dx\,dy$ and $(u,v) = \iint_\Omega uv\,dx\,dy$. It is convenient to model the wells using point-sources and -sinks represented by delta functions, i.e

$$q_1(\mathbf{x},t) = \sum_{wells} q_n(t)\delta(x-x_n, y-y_n). \tag{11}$$

We discretize the problem (10)-(11) using a standard finite element method (FEM). Due to the singularities present, special treatment is necessary to obtain an accurate discrete approximation. Analytic removal of the singularities has been proposed, [9], but will generally necessitate global modifications of the discrete equations. A promising alternative seems to be local mesh refinement of the well regions, [3]. Also the behavior of the tensor $\mathbf{A}(\mathbf{x})$, reflecting properties of reservoir rock and fluid mixtures, may offer potential for local mesh refinement.

We have chosen a refinement scheme where regular substructures are superimposed over the critical regions of a global regular mesh. This approach permits us to work

solely on regular mesh problems, treating the composite mesh within the framework of some global iterative method like the FAC solution strategy of McCormick et.al, [8], or the preconditioner concept of Bramble et.al, [3]. This patch refinement strategy also has the advantage that it can relatively easy be integrated into existing large scale codes.

Having solved equation (10) and determined the discrete pressure approximation, p_h, in the space of functions that are linear when restricted to an element of the composite grid of Figure 1, our next task is to find the velocity. Straightforward differentiation of the pressure approximation leaves us with velocity components that are constant on each element, giving a discretization error of the order of the mesh size.

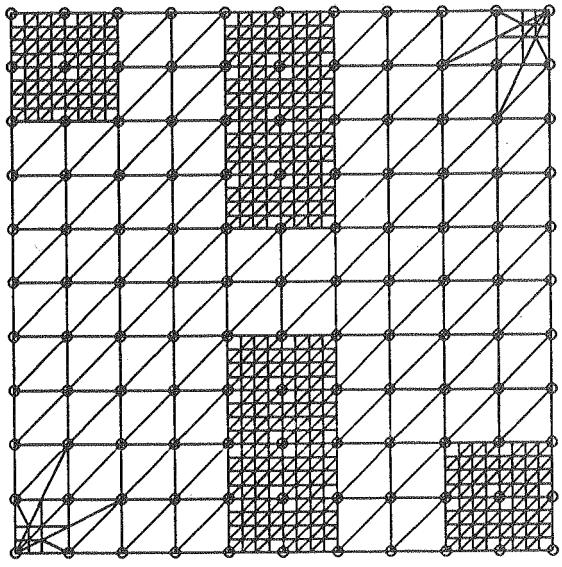

Figure 1: Typical composite mesh for pressure and velocity computations.

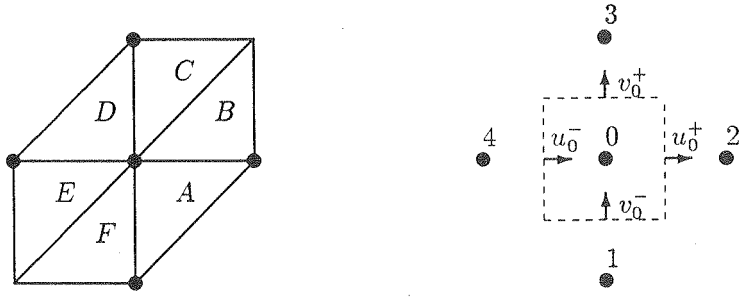

Figure 2: a) Support of local test function. b) Node ordering and control volume.

Instead we consider the following algorithm. The discrete version of (10) associated with the node "0" of Figure 2, can be written:

$$A(p_h, \phi_h^0) = (\tfrac{1}{2}(a_A + a_B)\tfrac{p_0 - p_2}{\Delta x} + \tfrac{1}{2}(a_D + a_E)\tfrac{p_0 - p_4}{\Delta x})\Delta y + (\tfrac{1}{2}(b_C + b_D)\tfrac{p_0 - p_3}{\Delta y} + \tfrac{1}{2}(b_A + b_F)\tfrac{p_0 - p_1}{\Delta y})\Delta x, \quad (12)$$

where ϕ_h^0 is the local test function, $a_A, \ldots, b_F$ are the components of $\mathbf{A} = a\mathbf{ii} + b\mathbf{jj}$ averaged over the different elements of Figure 2(a), p_i is the pressure at node i of Figure 2(b) and Δx and Δy are the mesh sizes. Due to equation (2), which defines the Darcy velocity, equation (12) has a natural interpretation in terms of the fluxes through the edges of a control volume surrounding the node 0 of Figure 2(b). That is, equation (12) may be written in the form

$$A(p_h, \phi_h^0) = (u_0^+ - u_0^-)\Delta y + (v_0^+ - v_0^-)\Delta x, \quad (13)$$

see Figure 2(b). By linear interpolation, the fluxes determine a unique velocity for each node (Figure 3):

$$u_i = \frac{1}{2}(u_i^+ + u_i^-) \text{ and } v_i = \frac{1}{2}(v_i^+ + v_i^-), \quad i = 1, ..., 4, \quad (14)$$

where of course $u_1^+ = u_2^-$ etc. These nodal values then define continuous and piecewise

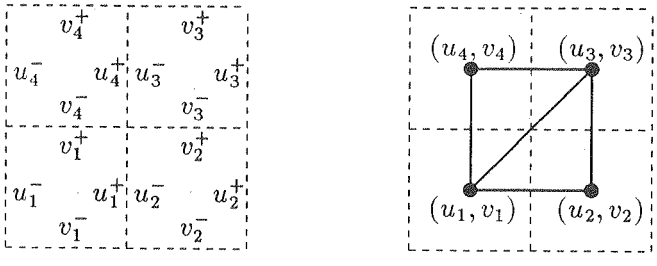

Figure 3: (a) Four adjacent control volumes and the associated fluxes. (b) Piecewise linear velocity components.

linear approximations to the velocity components. Conservation of mass for the control volumes is a direct consequence of equation (13), and leads to similar conservation properties for the modified velocity field. For example, by using (13) and (14) one obtains

$$\frac{1}{2}(v_1 + v_2)\Delta x + \frac{1}{2}(u_1 + u_4)\Delta y - \frac{1}{2}(v_4 + v_3)\Delta x - \frac{1}{2}(u_2 + u_3)\Delta y = 0, \quad (15)$$

i.e. flux conservation for the boldfaced rectangle of Figure 3(b).

The procedure outlined above resembles the approach used to improve the accuracy of the gradient computed from a finite element approximation, see [7]. A proof similar to that of [7] seems to carry through also for our algorithm, indicating discrete velocity components of second order accuracy in the mesh size for a uniform mesh. This has so far been confirmed by the numerical investigations.

The concept of control volumes and flux conservation make the idea convenient for generalization to the case of local mesh refinement. We have implemented an algorithm handling composite meshes like that of Figure 5, and a thorough discussion of this aspect is given in [10].

3 Saturation.

Due to the small parameter ϵ, the parabolic equation (3) has an almost hyperbolic nature. Consequently, it is common to limit the study of this equation to the pure convection problem

$$\phi \frac{\partial}{\partial t} S + \mathbf{v} \cdot \nabla f(S) = 0. \tag{16}$$

The s-shaped form of typical fractional flow functions, $f(S)$, may cause equation (16) to develop nonunique solutions.

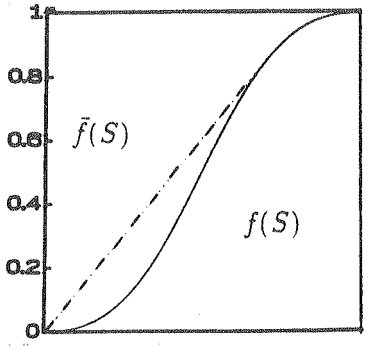

Figure 4: The fractional flow function and its convex hull.

In order to obtain uniqueness, the entropy and shock conditions are imposed on equation (16). We shall be concerned with the transport of a fully established shock. In this case, the shock condition is equivalent to replacing $f(S)$ in (16) by its convex hull, $\bar{f}(S)$, see Figure 4.

The operator splitting introduced by Espedal and Ewing, [5], takes advantage of this way of handling equation (16). Their algorithm aims at the complete equation (3), with the small but physically important diffusion term included. Let $S^m(\mathbf{x})$ be the approximation to $S(\mathbf{x}, t^m)$, the solution at time t^m. By the splitting

$$f(S) = \bar{f}(S) + b(S)S, \tag{17}$$

of the fractional flow function, and solution of the modified transport problem

$$\phi \frac{\partial}{\partial t} \bar{S}^{m+1} + \mathbf{v} \cdot \nabla \bar{f}(\bar{S}^{m+1}) = 0, \quad \bar{S}^{m+1}(\mathbf{x}, t^m) = S^m(\mathbf{x}), \quad t \in [t^m, t^{m+1}], \tag{18}$$

a first approximation, $\bar{S}^{m+1}(\mathbf{x}) \equiv \bar{S}^{m+1}(\mathbf{x}, t^{m+1})$, to the saturation $S(\mathbf{x}, t^{m+1})$, is achieved.

Equation (3) is then discretized in time and linearised by expanding it with respect to $\bar{S}^{m+1}(\mathbf{x})$. Neglecting terms of $O(\Delta t \epsilon)$, we get (see [5])

$$S^{m+1} + \frac{\Delta t}{\phi} \nabla \cdot (\mathbf{v} b(\mathbf{x}) S^{m+1}) - \frac{\Delta t \epsilon}{\phi} \nabla \cdot (\mathbf{D}(\mathbf{x}) \cdot \nabla S^{m+1}) = \bar{S}^{m+1}(\mathbf{x}), \tag{19}$$

where $b(\mathbf{x}) = b(\bar{S}^{m+1}(\mathbf{x}), \mathbf{x})$, $\mathbf{D}(\mathbf{x}) = \mathbf{D}(\bar{S}^{m+1}(\mathbf{x}), \mathbf{x})$, and $\Delta t = t^{m+1} - t^m$. This gives an improved approximation, $S^{m+1}(\mathbf{x})$, to the solution $S(\mathbf{x}, t^{m+1})$.

The localized shock region leaves us with a two scale problem, well suited for adaptive local refinement in space. Figure 5 shows a typical solution and a convenient computational grid.

Let $\mathbf{S}_h^m(\Omega)$ be the space of functions on Ω that are bilinear when restricted to an element of the composite grid associated with time level t^m. Starting out with $S_h^m \in \mathbf{S}_h^m(\Omega)$, where S_h^m is the discrete approximation to $S^m(\mathbf{x})$, we solve (18) using the modified method of characteristics. We first update the coarse nodes, and then decide where the grid should be refined by scanning the coarse grid information. In this way the discrete space $\mathbf{S}_h^{m+1}(\Omega)$ and the discrete approximation $\bar{S}_h^{m+1}$ are determined simultaneously.

To obtain a stable discrete solution we have used a Petrov-Galerkin procedure to discretize equation (19) with $\mathbf{S}_h^{m+1}(\Omega)$ as the trial space. Appropriate test functions

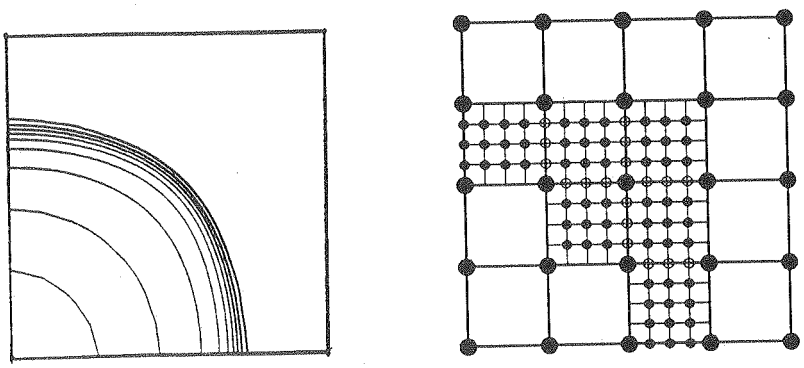

Figure 5: Typical solution and the composite grid used in the computations.

can then be determined by a symmetrization technique developed by Barrett and Morton, [1]. For the given problem it can be shown that the test-functions introduced by Heinrich et. al. [6], form a suitable test space. Using (9) as boundary condition, we get the discrete Galerkin equations:

$$\begin{aligned} A(S_h^{m+1},\psi) \equiv\ & (S_h^{m+1},\psi) - (\tfrac{\Delta t}{\psi}\mathbf{v}b S_h^{m+1},\nabla\psi) + (\epsilon\tfrac{\Delta t}{\psi}\mathbf{D}\cdot\nabla S_h^{m+1},\nabla\psi) \\ =\ & (\bar{S}_h^{m+1},\psi), \qquad \forall\,\psi \in \mathbf{T}_h^{m+1}(\Omega). \end{aligned} \tag{20}$$

The discrete test space at time level t^{m+1}, $\mathbf{T}_h^{m+1}(\Omega)$, consists of those functions on Ω which restricted to an element of the composite grid are linear combinations of the following basic functions (see Figure 6):

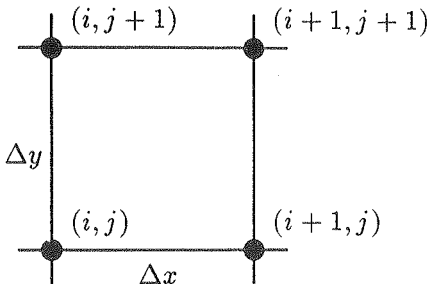

Figure 6: Element of the composite grid.

$$\psi_i^j(\mathbf{x}) = (\frac{x_{i+1}-x}{\Delta x} + c^x\frac{(x-x_i)(x_{i+1}-x)}{\Delta x^2})(\frac{y_{j+1}-y}{\Delta y} + c^y\frac{(y-y_j)(y_{j+1}-y)}{\Delta y^2}) \quad (21)$$

$$\psi_{i+1}^j(\mathbf{x}) = (\frac{x-x_i}{\Delta x} - c^x\frac{(x-x_i)(x_{i+1}-x)}{\Delta x^2})(\frac{y_{j+1}-y}{\Delta y} + c^y\frac{(y-y_j)(y_{j+1}-y)}{\Delta y^2}) \quad (22)$$

$$\psi_i^{j+1}(\mathbf{x}) = (\frac{x_{i+1}-x}{\Delta x} + c^x\frac{(x-x_i)(x_{i+1}-x)}{\Delta x^2})(\frac{y-y_j}{\Delta y} - c^y\frac{(y-y_j)(y_{j+1}-y)}{\Delta y^2}) \quad (23)$$

$$\psi_{i+1}^{j+1}(\mathbf{x}) = (\frac{x-x_i}{\Delta x} - c^x\frac{(x-x_i)(x_{i+1}-x)}{\Delta x^2})(\frac{y-y_j}{\Delta y} - c^y\frac{(y-y_j)(y_{j+1}-y)}{\Delta y^2}) \quad (24)$$

where

$$c^\eta = 3(\frac{2}{\beta^\eta} - \coth(\frac{\beta^\eta}{2})),\ \eta = x, y. \quad (25)$$

We note that the mesh Peclet numbers $\beta^x = bv^x\Delta x/\epsilon d_{11}$ and $\beta^y = bv^y\Delta y/\epsilon d_{22}$ depends on the components of the velocity field $\mathbf{v} = v^x\mathbf{i} + v^y\mathbf{j}$, the diffusion tensor $\mathbf{D} = d_{11}\mathbf{ii} + d_{22}\mathbf{jj}$ and the convective term $b(S)$ as defined by equation (17).

To construct a preconditioner for the resulting linear system, we have used the ideas of the BEPS-preconditioner of Bramble et.al [3]. We have combined this with the DD1-preconditioner of Bramble et.al, [2], in order to break down the complex of refined blocks, see Figure 5. Each refined block will then be a subdomain in the DD1 sense, see also [4]. Some modifications related to the non-symmetric nature of the problem is necessary:

- Consider the coarse grid problem assigning "coarse-nodes-values" for the inverse action of the preconditioner (step 2 of BEPS). Over the region of refined blocks, we have taken the test functions on the coarse mesh to be linear combinations of the fine mesh test functions, i.e the test functions constructed from eqs. (21)-(24) using the fine mesh. This is convenient when computing data for the coarse grid problem and consistent with the composite grid operator.

- On the edges between refined subdomains we consider the coupling along the edge given by the composite operator. Using the coarse node values as boundary conditions, we solve a one dimensional boundary value problem to assign values to the nodes along the edge. This process replaces the linear extension between the coarse nodes (cf. step 3 of DD1) and the zero-Dirichlet problem along each edge (step 2 of DD1), a procedure that proved difficult to adapt to the nonsymmetric case.

4 Numerical experiments.

In order to solve the linear system arising from equation (20), we use the preconditioner defined in the ORTHOMIN algorithm as given by Vinsome [11]. For the computations presented here, we have chosen to restart the orthogonalization procedure after each 7th iteration.

Model spesification: We have used the following computational forms of the coefficients: $\phi = .2$, $k_x = k_y = 1$, $\lambda_w = S^2$, $\lambda_o = (1-S)^2$ and $\mathbf{D} = S(1-S)(\mathbf{ii}+\mathbf{jj})$. The well rates needed in equation (11), are set to $q(t) = \pm.25$ for injectors and producers respectively. We choose our domain Ω to be the unit rectangle with an injector in the lower left corner and a producer in the upper right corner, i.e. we consider the diagonal grid of the five-spot pattern. The initial condition for the saturation equation is given as an approximately established shock somewhat away from the injector.

To check for grid orientation effects the diagonal grid computations has been compared with equivalent computations on a parallel grid. As we expected, the modified method of characteristics produced only negligible grid effects.

We measure time as the ratio between the amount of water injected and the total pore volume available. The elapsed time and the time-step will be denoted t_{PVI} and Δt_{PVI} respectively. The domain Ω is partitioned into $n_C \times n_C$ coarse elements and each refined block is divided into $n_R \times n_R$ fine elements, see Figure 5. We give the residual r_0 obtained when $\bar{S}_h^{m+1}$ is used as initial approximation to S_h^{m+1}, and the average reduction factor, q, observed during the iterative process. We also report the number of iterations required to reduce r_0 to a tolerance set to 10^{-5}. N denotes the total number of degrees of freedom associated with the composite grid. The mass balance (mb) is the ratio between the amount of water in the reservoir as given by the saturation solution, and the amount of water injected.

Local refinement: For the relatively large diffusion parameter of Figure 7, we see that the solution, for the mesh-sizes used, is invariant to increased refinement down to a saturation level of about .5. This leads us to believe that we in this area succeed in modeling genuine physical diffusion. Below this level, the steep solution requires a very fine resolution. Considering the somewhat irregular appearance of Figure 7(c) and the mass balance column of table 1, we conclude that high resolution has its drawbacks. The computations also confirm the fact, see Bramble et. al. [2], that as the relative resolution of the refined blocks increases, a preconditioner of this type becomes less effective, see also Bramble et. al. [2].

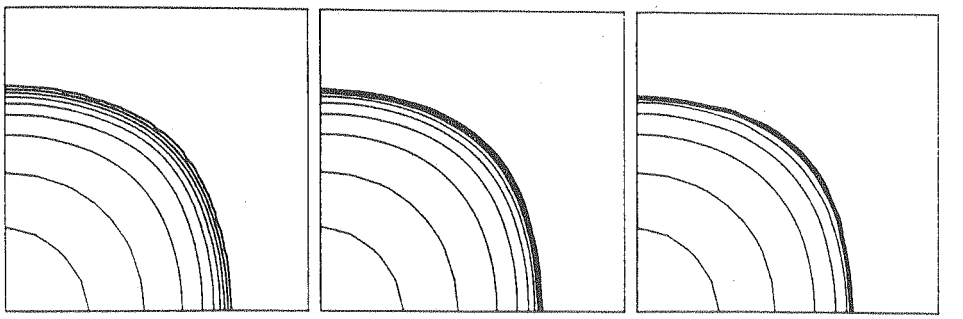

Figure 7: Saturation for different resolution of the front. $\epsilon = .01$, $\Delta t_{PVI} = .05$, $t_{PVI} = .32$ and $n_C = 10$. (a) $n_R = 5$ (b) $n_R = 10$ (c) $n_R = 20$

n_R	r_0	i	q	mb	N	fig.
5	1.20-3	7	.51	.994	801	Figure 7(a)
10	1.78-3	13	.67	.993	3001	Figure 7(b)
20	4.60-3	23	.76	.988	11103	Figure 7(c)

Table 1: Performance of the preconditioner for various resolutions of the front.

Effects of diffusion: Figure 8(a) depicts the pure Buckley-Leverett solution, and Figure 8 (b)-(c) and Figure 7(b) clearly demonstrate how the effect of increased diffusion introduce more structure into the solution. As the impact of the diffusion term increases, we see from table 2 that the characteristic solution become a slightly worse first approximation to the solution. Consequently more work is needed to obtain the corrected solution.

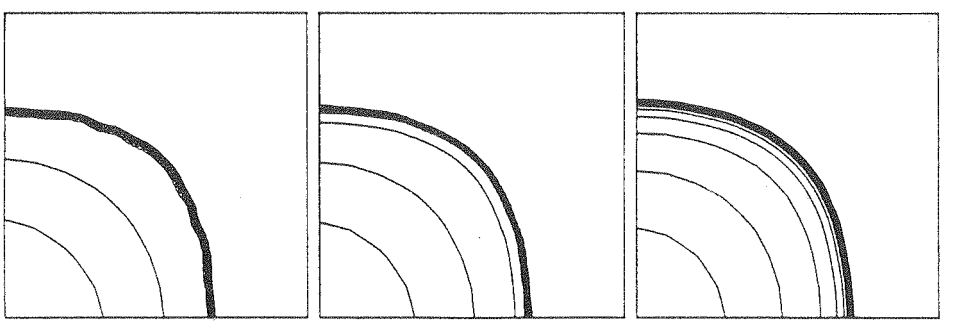

Figure 8: Saturation for different choices of the diffusion parameter. $n_R = 10$, $\Delta t_{PVI} = .05$, $t_{PVI} = .32$ and $n_C = 10$. (a) $\epsilon = .0$ (b) $\epsilon = .001$ (c) $\epsilon = .005$

ϵ	r_0	i	q	mb	N	fig.
.001	3.05-4	5	.48	.992	1687	Figure 8(b)
.005	1.01-3	10	.63	.992	2389	Figure 8(c)
.010	1.78-3	13	.67	.993	3001	Figure 7(b)

Table 2: Performance of the preconditioner for various diffusion parameters.

References

[1] J.W. Barrett and K.W. Morton. Approximate symmetrization and Petrov-Galerkin methods for diffusion-convection problems.
Comp. Meth. in Appl. Mech. and Eng. 45 (1984) 97-122 North Holland

[2] J.H. Bramble, J.E. Pasciak and A.H. Schatz. The construction of preconditioners for elliptic problems by substructuring.
J. Math. Comp. 47 (1986) 103-134

[3] J.H. Bramble, R.E. Ewing, J.E. Pasciak and A.H. Schatz. A preconditioning technique for the efficient solution of problems with local grid refinement.
Comp. Meth. in Appl. Mech. and Eng. 67 (1988) 149-159 North Holland

[4] H.K. Dahle, M.S. Espedal, R.E. Ewing and O. Sævareid. Characteristic Adaptive Sub-domain Methods for Reservoir Flow Problems.
To be published in Numerical Methods for Partial Differential Equations.

[5] M.S. Espedal and R.E. Ewing. Characteristic Petrov-Galerkin subdomain methods for two-phase immiscible flow.
Comp. Meth. in Appl. Mech. and Eng. 64 (1987) 113-135 North Holland

[6] J.C. Heinrich, P.S. Huyakorn, A. R. Mitchell and O. C. Zienkiewicz. An upwind finite element scheme for two-dimensional convective transport equations.
Inter. J. Numer. Engrg. 11 (1977) 131-143

[7] M. Křižek and P. Neittanmäki. Superconvergence Phenomenon in the Finite Element Method Arising from Averaging Gradients.
Numer. Math., **45**. 105-116 (1984).

[8] S. McCormick and J.W. Thomas. The Fast Adaptive Composite Grid (FAC) Method for Elliptic Equations.
Math. of Comp., **46(176)**. 439-456 (1986).

[9] T.F. Russel and M.F. Wheeler. Finite Element and Finite Difference Methods for Continuous Flows in Porous Media.
The Mathematics of Reservoir Simulation, (R.E. Ewing, ed.) SIAM, Philadelphia, PA, 1983.

[10] O. Sævareid. Local Mesh Refinement for Reservoir Flow Problems.
To be published.

[11] P.K.W. Vinsome. ORTHOMIN, an iterative method for solving sparse banded sets of simultaneous linear equations.
Paper no. SPE 5729, Proceedings of Fourth SPE Symposium on Numerical Simulation, Los Angeles, California, 1976.